Thermophysical properties of dry and humid air by molecular simulation including dew point calculations with the Mollier ensemble

Bernhard Eckl[1], Thorsten Schnabel[1], Jadran Vrabec[2]*,
Martin Wendland[3], and Hans Hasse[4]

[1]Institut für Technische Thermodynamik und Thermische Verfahrenstechnik, Universität Stuttgart, Pfaffenwaldring 9, 70550 Stuttgart, Germany

[2] Lehrstuhl für Thermodynamik und Energietechnik, Universität Paderborn, Warburger Straße 100, 33098 Paderborn, Germany

[3]Institut für Verfahrens- und Energietechnik, Universität für Bodenkultur Wien, Muthgasse 107, 1190 Wien, Austria

[4] Lehrstuhl für Thermodynamik, Technische Universität Kaiserslautern, Erwin-Schrödinger-Straße 44, 67663 Kaiserslautern, Germany

Abstract

A pseudo-ensemble, the Mollier ensemble, is proposed for the dew point calculation of humid air systems. This approach combines features of the isobaric-isothermal (NpT) ensemble and the grand-canonical (μVT) ensemble. The molecular model for dry air is taken from previous work and compared to experimental data as well as to two recommended reference quality equations of state regarding vapor-liquid equilibria, thermal, and caloric properties. An excellent agreement is found for temperatures up to 1000 °C and pressures up to 200 MPa. For water, two different

*Tel.: +49-5251/60-2421, Fax: +49-5251/60-3522, Email: jadran.vrabec@upb.de

molecular models are considered, the popular TIP4P model from the literature and an optimized version that better describes the vapor pressure. Both water models are used in combination with the molecular dry air model to predict the compressed gas density as well as the dew point of humid air at 60 and 80 °C for elevated pressures up to 25 MPa. The results are in very good agreement with experimental data from the literature.

Keywords: Molecular simulation; Mollier ensemble; dew point; compressed humid air; dry air model

1 Introduction

Thermophysical fluid property modeling is crucial for the design and optimization of many technical processes in power generation and process engineering. Knowledge on thermodynamic data of compressed humid air and other compressed humid gases are needed for technical applications, e.g., humid gas turbine, compressed air energy storage, or carbon dioxide separation and sequestration, while only little experimental data is available [1]. Of special interest is the dew point of compressed humid air, where significant deviations from ideal gas properties are reported in the literature [2, 3, 4, 5, 6, 7]. Molecular modeling and simulation opens new perspectives in the prediction of thermophysical properties, since molecular models are able to closely and consistently mimic structure, dynamics, and energetics in fluids and are thus superior to classical phenomenological approaches. As a consequence, molecular models are well suited, e.g., for predictions of thermodynamic properties of humid air.

The dew point of humid air is often characterized by the partial pressure of water $p_\mathrm{W} = x_\mathrm{W} \cdot p$ in the compressed gas at saturation, where x_W is the water mole fraction. The water content of humid air increases at constant temperature progressively with total pressure p due to an increasing influence of the intermolecular interactions in the gas phase and due to the compression of the liquid phase. This effect can be described by the vapor pressure enhancement

factor

$$f_{\mathrm{W}}(T,p) = \frac{p_{\mathrm{W}}}{p^0_{\mathrm{W}}} \ , \tag{1}$$

which is the ratio of the partial pressure of water p_{W} to the vapor pressure of pure water p^0_{W} at the same temperature T. The vapor pressure enhancement factor f_{W} is measured via the mole fraction x_{W} of water in the saturated gas phase either by gas-chromatography or gravimetrically after expansion. Data for f_{W} is very sensitive to experimental errors and uncertainties in the determination of the mole fraction so that f_{W} data from gas-chromatography is often inconsistent. The gravimetric method is more suitable but very elaborate [8].

The dew point of compressed humid gases can also be described in terms of the vapor concentration enhancement factor [6, 7]

$$g_{\mathrm{W}}(T,p) = \frac{c_{\mathrm{W}}}{c^0_{\mathrm{W}}} \ , \tag{2}$$

which is the ratio of the water concentration $c_{\mathrm{W}} = x_{\mathrm{W}} \cdot \rho$ in the saturated humid gas to the saturated vapor density of pure water c^0_{W}. The water concentration c_{W} can directly be measured by spectrometry. This was recently used by one of us, cf. Koglbauer and Wendland [7, 9], who developed a new method to measure g_{W} by FTIR spectrometry. This method yields consistent data over a wide range of temperature and pressure. Data on g_{W} of compressed humid air [7], humid nitrogen, humid argon, and humid carbon dioxide [9] agree qualitatively well with literature data on f_{W} as far as available. However, a quantitative comparison relies on gas densities that are needed for the conversion between both enhancement factors. They are related by [6, 7]

$$g_{\mathrm{W}} = f_{\mathrm{W}} \frac{Z^0_{\mathrm{W}}}{Z} \ , \tag{3}$$

where Z and Z^0_{W} are the compressibility factors of saturated humid gas and pure water vapor, respectively.

The vapor pressure enhancement factor can be calculated from an equation of state (EOS) via an extension of Raoult's law [8]

$$f_{\mathrm{W}}(T,p) = \frac{\phi^0_{\mathrm{W}}}{\phi_{\mathrm{W}}} \exp\left(\int_{p^0_{\mathrm{W}}}^{p} \frac{v_{\mathrm{W}}}{kT}\mathrm{d}p\right) (1 - x_{\mathrm{G}}) \ . \tag{4}$$

The first term considers the gas phase non-ideality via the fugacity of pure saturated water vapor ϕ^0_{W} and the fugacity of water at the dew point of humid air ϕ_{W} which are usually determined from virial EOS. The second and third terms are due to the liquid phase. The Poynting correction considers the isothermal compressibility of pure liquid water and the expression $(1 - x_{\mathrm{G}})$ is due to the gas mole fraction x_{G} in aqueous solution. The isothermal compressibility contributes considerably to f_{W}, while the gas solubility has a very small effect.

A comparison of the experimental g_{W} data for humid air by Koglbauer and Wendland [7] with values by Wiley and Fisher [6], calculated by a virial EOS model fitted to the experimental f_{W} data, shows some deviations at elevated pressures which will be discussed subsequently. Also recent humid air density data deviates from virial EOS models [1, 10]. The suitability of virial EOS for the dew point of highly compressed humid gases has been contested elsewhere [8] and the application of empirical multi-parameter equations of state was suggested. But these need a large and reliable data base for their development which is not available yet.

It can be concluded that it is important to gain insight in the behavior of compressed humid air and to determine additional thermodynamic data from an independent source such as molecular simulation for comparison with experimental results and for the development of new models. Molecular simulation may simultaneously yield consistent data on f_{W}, g_{W}, saturated gas density, etc.

The present paper is organized in two parts. Firstly, a molecular model for dry air, proposed in earlier work [11, 12], is assessed regarding thermal and caloric properties, i.e. density and internal energy, for temperatures up to 1000 °C and pressures up to 200 MPa. The simulation results are compared

to two reference EOS recommended by the National Institute of Standards and Technology.

In the second part, the dry air molecular model is combined with two different water models for the simulation of humid air. In addition to predictions of the density, dew point data of humid air are presented which were calculated by simulation using a new pseudo-ensemble. The simulation data is compared to experimental data and a conclusion is drawn. Finally, simulation details are given in the Appendix.

2 Dry air simulations

For the leading three dry air components nitrogen, oxygen, and argon, molecular models from previous work [13] were used. These models are based on the two-center Lennard-Jones plus quadrupole (2CLJQ) pair potential that has successfully been applied for the prediction of numerous binary and ternary vapor-liquid equilibria [11, 14, 15, 16, 17], the Joule-Thomson inversion curve of pure substances, natural gas mixtures, and air [12, 18] as well as transport properties [19, 20]. Due to their accuracy and numerical efficiency they have been used by other groups as well, e.g. regarding adsoption [21, 22] or fluid behavior inside carbon nanotubes [23, 24].

The interaction energy u_{ij} between two 2CLJQ molecular models writes as

$$u_{ij} = \sum_{a=1}^{2}\sum_{b=1}^{2} 4\varepsilon_{ij}\left[\left(\frac{\sigma_{ij}}{r_{ijab}}\right)^{12} - \left(\frac{\sigma_{ij}}{r_{ijab}}\right)^{6}\right] + \frac{Q_i Q_j}{4\pi\epsilon_0 r_{ij}^5} f(\boldsymbol{\omega}_i, \boldsymbol{\omega}_j) \ , \qquad (5)$$

where ε_{ij} and σ_{ij} are the energy and size parameter of the Lennard-Jones potential, respectively. r_{ijab} denotes the site-site distance between molecules i and j. Q_x is the quadrupole moment located in the center of mass of molecule x, while ϵ_0 is the permittivity of vacuum, and r_{ij} the center of mass distance. Finally, $f(\boldsymbol{\omega}_i, \boldsymbol{\omega}_j)$ describes the dependency of the quadrupolar interaction on the orientations $\boldsymbol{\omega}_x$, cf. [25]. The four (in case of argon two) state-independent pure

substance parameters have been adjusted in prior work [13] to experimental vapor pressure and saturated liquid density, cf. Table 1.

In case of mixtures, the parameters of the unlike Lennard-Jones interactions are determined by the modified Lorentz-Berthelot rule

$$\sigma_{ij} = \frac{\sigma_{ii} + \sigma_{jj}}{2} \ , \tag{6}$$

and

$$\varepsilon_{ij} = \xi \cdot \sqrt{\varepsilon_{ii}\varepsilon_{jj}} \ , \tag{7}$$

where σ_{xx} and ε_{xx} are the Lennard-Jones interaction parameters of the pure substances molecular models. ξ is a state-independent binary parameter which has been adjusted to a single binary vapor pressure of each binary subsystem. This approach was found to be superior to numerous combining rules from the literature [26].

The three binary interaction parameters for the dry air model were taken from prior work [11] on vapor-liquid equilibria of the binary subsystems, cf. Table 2. No further optimizations were made in the present work, thus all mixture data presented here are strictly predictive.

To predict the vapor-liquid equilibrium (VLE) by simulation for that ternary system, the Grand Equilibrium method was applied [27]. Technical details are given in the Appendix. Figure 1 shows the VLE simulation results in comparison to experimental data [28] and the results of the recent GERG-2004 EOS [29]. The simulation results are in excellent agreement with the experimental data. The GERG-2004 EOS deviates by about 3 to 4 mole % from the experimental and simulation data sets on both the bubble and the dew line towards the nitrogen-rich region which is somewhat more than the estimated uncertainty stated in [29].

The term "dry air" is used in the following for that ternary mixture at the composition found in nature: $x_{\mathrm{N2}} = 0.781438$ mol/mol, $x_{\mathrm{O2}} = 0.209540$

mol/mol, and $x_{\mathrm{A}r} = 0.009022$ mol/mol [7, 10], cf. Appendix. Figures 2 to 5 show simulation results for the density ρ and the residual internal energy $u^{\mathrm{res}} = u(T,p) - u(T,p \to 0)$ for dry air along isotherms and isobars, respectively, cf. Tables 3 and 4. Covering state points over a wide range, reaching up to 1000 °C and 200 MPa, the simulation results were compared to two EOS of reference quality, i.e. the GERG-2004 EOS [29] and the EOS by Lemmon et al. [30]. An excellent agreement between simulation and both EOS was found. Deviations to the GERG-2004 EOS are below 1.2% for the density and below 6% for the residual internal energy in all cases. The largest deviations for the residual internal energy were found at 1000 °C, where the two considered EOS deviate by up to 10% from each other. Present simulation results lie in between, however, they rather follow the trend of the EOS by Lemmon et al. [30] which was specifically developed for dry air.

3 Humid air simulations

3.1 Mollier ensemble

A pseudo-ensemble is proposed for the direct determination of the dew point of compressed humid air by molecular simulation. This approach, we would like to name it Mollier ensemble, combines features from the broadly used isobaric-isothermal (NpT) and grand-canonical (μVT) ensembles [31]. During simulation, the saturated gas phase is sampled at a specified temperature T and a specified total pressure p. Also specifying the number of dry air molecules, i.e. keeping the number of nitrogen, oxygen, and argon molecules constant, the water content is varied to achieve chemical equilibrium with the aqueous liquid phase. The Mollier ensemble has similarities with the "osmotic" pseudo-ensemble proposed by Escobedo [32, 33] which is based on earlier work of Mehta and Kofke [34]. In contrast to these works, the two phases in equilibrium are not simulated simultaneously, but subsequently which resembles the approach followed in the Grand Equilibrium method [27].

The fluid phase coexistence of the mixture water + air around ambient conditions is a typical example for gas solubility. The Henry's law constants of the three gaseous components in pure water at 80 °C are: $H_{\mathrm{N2}} \approx 10.5$ GPa, $H_{\mathrm{O2}} \approx 5.5$ GPa, and $H_{\mathrm{Ar}} \approx 5$ GPa [35]. Thus, the aqueous liquid phase contains only a small quantity of the gaseous components, the total mole fraction $x_{\mathrm{N2}}+x_{\mathrm{O2}}+x_{\mathrm{Ar}}$ is in the order of 10^{-3} mol/mol at 80 °C and 25 MPa. Therefore, the chemical potential of water is hardly affected by the presence of the air components. Note that for high temperatures, closer to the critical point of water, this assumption is not valid.

For saturated states the phase equilibrium conditions apply, i.e. temperature, pressure, and chemical potential of all components are equal in the corresponding phases. These conditions were exploited to construct the Mollier ensemble which allows to determine the dew point of humid air for a specified pair of T and p.

On the basis of the discussion above, it is assumed that the chemical potential of water μ_{W} in the liquid is not significantly influenced by the presence of a small fraction of dry air molecules. Then, the chemical potential of liquid water can be calculated by a pure substance NpT simulation at T and p in a first step. For liquid water around ambient conditions, sophisticated simulative methods, like the expanded ensemble [36, 37, 38], are needed to obtain entropic properties with reasonable statistical uncertainties. In the second step, a humid air dew point simulation with a specified number of air molecules $N_{\mathrm{N2}} + N_{\mathrm{O2}} + N_{\mathrm{Ar}}$ was performed, where T, p, and $\mu_{\mathrm{W}}(T, p)$ were also specified. Of course, in that pseudo-ensemble, the number of water molecules N_{W} and the volume of the vapor phase V must be allowed to fluctuate. Therefore, a Monte-Carlo scheme was employed here, cf. Appendix for details. The procedure is illustrated in Figure 12.

The chemical potential of water μ_{W}, taken from the pure liquid water run, was specified through insertion and deletion of water molecules during simulation of the vapor phase like in the standard μVT ensemble. The probability of

insertions and deletions is then determined by comparison between the resulting potential energy change and the desired residual chemical potential $\mu_{\mathrm{W}}^{\mathrm{res}}$. Note that $\mu_{\mathrm{W}}^{\mathrm{res}}$ is defined by subtracting the solely temperature dependent ideal part $\mu^{\mathrm{id}}(T)$ from the total chemical potential. The acceptance probability P_{acc} for a water molecule insertion writes as [31]

$$P_{acc}(N_{\mathrm{W}} \rightarrow N_{\mathrm{W}}{+}1) = \min\left(1,\ \frac{V}{N_{\mathrm{W}}+1} \cdot \exp\left\{\frac{\mu_{\mathrm{W}}^{\mathrm{res}} + [U(N) - U(N+1_{\mathrm{W}})]}{kT}\right\}\right), \tag{8}$$

where $U(N)$ and $U(N{+}1_{\mathrm{W}})$ denote the configurational energy of the system with a total number of N molecules and N plus one water molecule, respectively. The acceptance probability for the deletion of a water molecule writes accordingly [31]

$$P_{acc}(N_{\mathrm{W}} \rightarrow N_{\mathrm{W}}{-}1) = \min\left(1,\ \frac{N_{\mathrm{W}}}{V} \cdot \exp\left\{\frac{-\mu_{\mathrm{W}}^{\mathrm{res}} + [U(N) - U(N-1_{\mathrm{W}})]}{kT}\right\}\right). \tag{9}$$

Additionally, the pressure is controlled by sampling the volume like in the standard NpT ensemble. The probability of a volume displacement is then determined by comparison between the resulting potential energy change and the product of specified pressure and volume displacement. The acceptance probability for a volume displacement ΔV is given by [31]

$$P_{acc}(\Delta V) = \min\left(1,\ \left(\frac{V+\Delta V}{V}\right)^{N} \cdot \exp\left\{\frac{p\Delta V + [U(V+\Delta V) - U(V)]}{kT}\right\}\right). \tag{10}$$

Experience shows that a Mollier ensemble simulation moves rapidly into the vicinity of the dew point. This process occurs well within the equilibration period. During the production period, volume and mole fraction of water fluctuate around the dew point average which is exemplified in Figure 6.

An additional facilitating approximation can be used. The pressure depen-

dence of the chemical potential for water is

$$\mu_{\mathrm{W}}(T,p) = \mu_{\mathrm{W}}(T,p^{\sigma}) + \int_{p^{\sigma}}^{p} \left(\frac{\partial \mu_{\mathrm{W}}}{\partial p}\right)_{T} \mathrm{d}p = \mu_{\mathrm{W}}(T,p^{\sigma}) + \int_{p^{\sigma}}^{p} v_{\mathrm{W}} \mathrm{d}p \ , \qquad (11)$$

where p^{σ} is some reference pressure, say the vapor pressure of pure water, and v_{W} denotes the volume of water. The integral can be approximated by a Taylor expansion around the reference pressure by [39]

$$\mu_{\mathrm{W}}(T,p) = \mu_{\mathrm{W}}(T,p^{\sigma}) + v_{\mathrm{W}}^{\sigma}(p-p^{\sigma}) - \frac{1}{2}\beta_{T,W} \cdot v_{\mathrm{W}}^{\sigma}(p-p^{\sigma})^2 + ... \ , \qquad (12)$$

where v_{W}^{σ} is the volume and $\beta_{T,W}^{\sigma}$ the isothermal compressibility, respectively, of liquid water at the reference pressure. These two properties are easily accessible in the NpT ensemble. The volume is simply

$$v = \frac{< V >}{N} \ , \qquad (13)$$

where the <> brackets denote the ensemble average. The isothermal compressibility may also conveniently be obtained in the NpT ensemble from volume fluctuations

$$\beta_T = \frac{1}{kT} \cdot \frac{1}{< V >} \cdot \left[< V^2 > - < V >^2\right] \ . \qquad (14)$$

However, in prior work it was seen that a first order expansion is usually sufficient for moderate pressure extrapolations when the temperature is far below its critical value of the regarded component [27]. As a consequence, the simulation results of a single pure liquid water run can be used for dew point simulations at any given pressure p as long as the approximation above holds.

3.2 Molecular models for water

For water, two different molecular models were used here. Firstly, the TIP4P model from Jorgensen et al. [40] was used. It consists of four interaction sites, one Lennard-Jones site located at the oxygen nucleus and three eccentric partial

charges to account for hydrogen bonding and the electrostatic interactions. All sites are situated in a plane, cf. Figure 7. The TIP4P model has been parameterized to reproduce the VLE of pure water [40], the model parameters are listed in Table 5. However, it shows significant deviations from experimental data for vapor pressure and saturated vapor density which will be discussed below in more detail.

Thus, the TIP4P water model was reparameterized here, keeping the original number of interaction sites. The model parameters were simultaneously adjusted to experimental data on vapor pressure, saturated liquid density, and enthalpy of vaporization of pure water. However, the main focus was on a good description of the vapor pressure. The optimized parameters of the new water model are listed in Table 5. Figures 8 to 10 show saturated densities, vapor pressure, and enthalpy of vaporization for the original TIP4P model and the new water model compared to experimental data [41]. The simulation data for the original TIP4P model were taken from Lísal et al. [42].

Figure 11 shows the deviations of the simulation data for both water models from experimental data for saturated liquid density, vapor pressure, and enthalpy of vaporization. The simulation results for the original TIP4P model yield mean unsigned errors in the range from triple point to critical point compared to experimental VLE data of 42, 9, and 15% for vapor pressure, saturated liquid density, and enthalpy of vaporization, respectively, while the new water model yields 21, 3, and 8%. Full numerical simulation results for the new water model are given in [43].

3.3 Homogeneous humid air

Klingenberg and Ulbig [10] recently published experimental data on the density of humid air at different state points and different water contents. In the present work, the dry air model was combined with the two discussed molecular models for water to predict the density of humid air and compare it to the results from [10]. For the unlike Lennard-Jones parameters, the standard Lorentz-Berthelot

mixing rule was applied, i.e. no additional binary interaction parameters were introduced and ξ was set to unity for all unlike interactions with water, cf. Equations (6) and (7). Thus, present humid air simulations are fully predictive.

Table 6 lists the simulation results, having an average statistical uncertainty of only about 0.3%, in comparison with experimental data [10]. A very good agreement was found as the deviations are below 2.5% for both water models. There is only a very moderate influence of the chosen water model on the quality of the results. Note that the deviations of the experimental density data from the present simulations are very similar to their deviations from EOS models [1].

3.4 Dew point of humid air

The dew point of humid air was calculated using the Mollier ensemble for two isotherms at six pressure levels. The same two quaternary molecular models, differing only in the water model, were used as for the homogeneous humid air simulations. For comparison with experimental data, the vapor pressure enhancement factor f_{W} and the vapor concentration enhancement factor g_{W} were determined, cf. Equations (1) and (2).

The equilibrium properties of pure water at the given temperature, i.e. vapor pressure p^0_{W} and saturated vapor concentration c^0_{W} being identical to the saturated vapor density ρ'', were determined in additional VLE simulations for pure water. This was done for both employed water models and the results are given in Table 7. Simulation details are briefly discussed in the Appendix.

From the Mollier ensemble simulations, the molar fraction of water x_{W} and the molar density at the dew point ρ were determined, cf. Table 8. The partial pressure of water $p_{\mathrm{W}} = x_{\mathrm{W}} \cdot p$ and the vapor concentration $c_{\mathrm{W}} = x_{\mathrm{W}} \cdot \rho$ in humid air can easily be calculated from these.

Figures 13 and 14 show the results for the vapor pressure and vapor concentration enhancement factors, respectively, in comparison to literature data taken from Wiley and Fisher [6], Koglbauer and Wendland [7] as well as the

GERG-2004 EOS [29]. Wiley and Fisher provide experimental data on f_W taken by a gravimetric method and Koglbauer and Wendland provide experimental data on g_W taken by FTIR spectrometry. Wiley and Fisher also give results for g_W predicted with a virial EOS model which they used to correlate their f_W data and that does not compare well to the experimental data by Koglbauer and Wendland below 80 °C (see [7]). Table 8 compiles the present data in numerical form.

For both water models, the simulation data for vapor pressure enhancement factor and vapor concentration enhancement factor is in agreement with the two data sets from [6, 7] almost throughout within their statistical uncertainties. However, the results with the newly developed water model yield a somewhat better agreement. In case of f_W, cf. Figure 13, both water models are above the correlation of Wylie and Fishers data [6]. At 60 °C, the new water model represents Wiley and Fishers data within the statistical uncertainty and the TIP4P model yields too high results, while at 80 °C both water models overestimate f_W for pressures above 10 MPa, cf. Figure 13. The GERG-2004 EOS [29] yields a significantly higher vapor pressure enhancement factor, which is more pronounced at the lower temperature.

Regarding the vapor concentration enhancement factor g_W, experimental data by Koglbauer and Wendland [7] and the model of Wylie and Fisher [6] deviate significantly for 60 °C. Molecular simulation yields results that are in between these data sets and agree with both within their statistical uncertainty. At 80 °C, the data sets from the two sources agree quite well with each other, while simulation predicts somewhat higher values. The results from the new water model agree with both sources within the statistical uncertainty, except for 25 MPa, while the TIP4P model yields too high results for g_W for pressures above 10 MPa, cf. Figure 14. Again, the GERG-2004 EOS [29] lies significantly above all other vapor concentration enhancement factor data sets regarded in this work.

4 Conclusion

Molecular modeling and simulation was applied to predict thermodynamic properties of humid air. In addition to densities of humid air in the homogeneous region, the dew point at 60 and 80 °C for different pressures up to 25 MPa was predicted.

For the dry air components nitrogen, oxygen, and argon, a ternary molecular model from prior work was taken. This molecular model was assessed regarding the ternary VLE as well as density and residual internal energy of dry air over a wide range of states in the homogeneous gaseous region. Very good results were obtained compared to experimental data and two reference EOS. Generally the deviations are a few percent or below.

For water, two different molecular models were used in the present work: firstly, the TIP4P model proposed by Jorgensen et al. and, secondly, a reparameterized version was optimized primarily to the experimental vapor pressure of pure water. Both water models were combined subsequently with the dry air model to simulate humid air. As no further parameters were introduced, the present humid air results are fully predictive.

The humid air density was predicted at different state points and water contents. The results were compared to recent experimental data, yielding deviations below 2.5% at the highest water mole fraction.

Finally, the dew point of humid air was predicted using the newly developed Mollier ensemble. The dew point results were also expressed in terms of the vapor pressure enhancement factor f_{W} and the vapor concentration enhancement factor g_{W}. Compared with experimental data, a satisfactory agreement was obtained for both water models. With both water models, vapor pressure and concentration enhancement in humid air may adequately be predicted. The new water model is quantitatively correct within its statistical uncertainties in most cases, deviations are below 17% for f_{W} and 15% for g_{W}. Compared to the GERG-2004 EOS, molecular modelling and simulation was found to be superior

with respect to these dew point properties.

5 Acknowledgment

The authors gratefully acknowledge financial support by Deutsche Forschungsgemeinschaft. The simulations are performed on the national super computer NEC SX-8 at the High Performance Computing Center Stuttgart (HLRS) and on the HP X6000 super computer at the Steinbuch Centre for Computing, Karlsruhe.

We would like to thank Anupam Srivastava for setting up and running the presented simulations for dry air.

6 Appendix

6.1 Dry air simulations

The Grand Equilibrium method [27] was used to calculate VLE data of dry air at 120 K. For the liquid phase, molecular dynamics (MD) simulations were performed in the NpT ensemble using isokinetic velocity scaling [25] and Anderson's barostat [44]. The number of molecules was $N = 864$ throughout and the time step was 1.18 fs. Starting from a face centered cubic (fcc) lattice as initial configuration, the fluid was equilibrated over 25 000 time steps with the first 5 000 time steps in the canonical (NVT) ensemble. The subsequent production period was 200 000 time steps with a membrane mass of 10^8 kg/m^4. Widom's insertion method [45] was applied to determine the chemical potential by inserting 3 456 test molecules for each species every production time step.

For the corresponding vapor, Monte Carlo (MC) simulations in the pseudo-μVT ensemble were performed. The simulation volume was adjusted to lead to an average number of 500 molecules in the vapor phase. After 1 000 initial NVT MC cycles, starting from a fcc lattice, 20 000 equilibration cycles in the pseudo-μVT ensemble were performed. The production run was sampled over

100 000 cycles. One MC cycle contained N attempts to displace and N attempts to rotate molecules, where N is the actual number of molecules, plus three insertion and three deletion attempts.

The cut-off radius was set to 17.5 Å throughout and a center of mass cut-off scheme was employed. Lennard-Jones long-range interactions beyond the cut-off radius were corrected employing angle averaging as proposed by Lustig [46]. The quadrupolar interactions of nitrogen and oxygen were not long-range corrected as their angle average vanishes [47]. Statistical uncertainties of all simulation results were estimated by a block averaging method [48].

For the homogeneous dry air simulations, MD was applied with the same technical details as used for the saturated liquid run, except that the chemical potential was not determined. It was aimed for a composition of air close to experimental data sources being $x_{\mathrm{N2}} = 0.781438$ mol/mol, $x_{\mathrm{O2}} = 0.209540$ mol/mol, and $x_{\mathrm{A}r} = 0.009022$ mol/mol [7, 10], which translates due to the finite total number of simulated molecules $N_{\mathrm{N2}} = 675$, $N_{\mathrm{O2}} = 181$, and $N_{\mathrm{A}r} = 8$ in case of $N = 864$. The effective composition was then $x_{\mathrm{N2}} = 0.78125$ mol/mol, $x_{\mathrm{O2}} = 0.20949$ mol/mol, and $x_{\mathrm{A}r} = 0.00926$ mol/mol.

6.2 Pure water and humid air simulations

During the optimization process of the new water model, the Grand Equilibrium method [27] was applied to calculate the VLE at seven temperatures from 300 to 600 K. Due to the well known difficulties of Widom's insertion method at the high liquid density of water, MC simulations were performed in the NpT ensemble for the liquid. The number of molecules was $N = 864$ and the chemical potential of water was determined by the gradual insertion method [38]. Starting from a fcc lattice, 15 000 Monte Carlo cycles were performed for equilibration and 50 000 for production, each cycle containing N translation moves, N rotation moves, and one volume move. Every 50 cycles, 5 000 fluctuating state change moves, 5 000 fluctuating particle translation/rotation moves, and 25 000 biased particle translation/rotation moves were attempted to measure

the chemical potential.

The vapor phase simulations were performed analogously to the dry air simulations described above, except that a larger number of 60 000 MC cycles was used for equilibration. This was done to better allow for the formation of hydrogen bonded water clusters in the vapor phase. The center of mass cut-off radius was 15.75 Å for liquid simulations and 17.5 Å for vapor simulations. The electrostatic interactions were corrected by the reaction field method [25].

The homogenous humid air simulations were done by MD. For production, 200 000 time steps of 1.18 fs were performed in the NpT ensemble.

To determine the dew point of humid air, pure liquid water simulations were done with both molecular water models at the specified temperature and the corresponding vapor pressure of water. The MC method was applied and gradual insertion was used to calculate the chemical potential of water in the pure liquid. Here, the same simulation details were used as for the saturated liquid simulations during the water model optimization.

The corresponding vapor (humid air) phase at the dew point was determined by MC simulations in the proposed Mollier ensemble. The number of molecules of the dry air components in the vapor phase was set to $N_{\mathrm{N2}}+N_{\mathrm{O2}}+N_{\mathrm{A}r} = 2\,000$ with an almost identical molecule number ratio as for the dry air simulations. In case of very low water mole fractions, the number of dry air molecules was increased to 4 000 to improve statistics. Again, starting from a fcc lattice, 15 000 Monte Carlo cycles were sampled for equilibration and 50 000 for production, each cycle containing N translation moves, N rotation moves, one volume move as well as two insertion and two deletion attempts of a water molecule, where N is the actual molecule number.

References

[1] Herrmann, S.; Kretzschmar, H.-J.; Teske, V.; Vogel, E.; Ulbig, P.; Span, R.; Gatley, D. Determination of Thermodynamic and Transport Properties of Humid Air for Power-Cycle Calculations. *PTB report* **2009**, submitted.

[2] Pollitzer, F.; Strebel, E. Über den Einfluss indifferenter Gase auf die Sattdampfkonzentration von Flüssigkeiten. *Z. Phys. Chem.* **1924**, *111*, 768.

[3] Webster, T. J. The effect on water pressure of superimposed air pressure. *J. Soc. Chem. Ind., London* **1950**, *69*, 343.

[4] Hyland, R. W.; Wexler, A. The enhancement of water vapor in carbon dioxide-free air at 30, 40, and 50 °C. *J. Res. Natl. Bur. Stand. A* **1973**, *77*, 115.

[5] Hyland, R. W. Correlation of the second interaction virial coefficients and enhancement factors for moist air. *J. Res. Natl. Bur. Stand. A* **1975**, *79*, 551.

[6] Wylie, R. G.; Fisher, R. S. Molecular interaction of water vapor and air. *J. Chem. Eng.* **1996**, *41*, 133.

[7] Koglbauer, G.; Wendland, M. Water vapor concentration enhancement in compressed humid air measured by Fourier transform infrared spectroscopy. *J. Chem. Eng. Data* **2007**, *52*, 1672.

[8] Wendland, M.; Koglbauer, G. Need of thermophysical data for the design and optimization of thermal processes. Preceedings of the 5th European Thermal-Sciences Conference, The Netherlands, 2008, CD-ROM, Keynote 6.

[9] Koglbauer, G.; Wendland, M. Water vapor concentration enhancement in compressed humid nitrogen, argon, and carbon dioxide measured by Fourier transform infrared spectroscopy. *J. Chem. Eng. Data* **2008**, *53*, 77.

[10] Klingenberg, G.; Ulbig, P. Isochoric pρT measurements on dry and humid air. *J. Chem. Eng. Data* **2007**, *52*, 1413.

[11] Vrabec, J.; Stoll, J.; Hasse, H. Molecular models of unlike interactions in fluid mixtures. *Mol. Sim.* **2005**, *31*, 215.

[12] Vrabec, J.; Kedia, G. K.; Hasse, H. Prediction of Joule-Thomson inversion curves for pure fluids and one mixture by molecular simulation. *Cryogenics* **2005**, *45*, 253.

[13] Vrabec, J.; Stoll, J.; Hasse, H. A set of molecular models for symmetric quadrupolar fluids. *J. Phys. Chem. B* **2001**, *105*, 12126.

[14] Stoll, J.; Vrabec, J.; Hasse, H. Vapor-liquid equilibria of mixtures containing nitrogen, oxygen, carbon dioxide, and ethane. *AIChE J.* **2003**, *49*, 2187.

[15] Vrabec, J.; Kedia, G. K.; Buchhauser, U.; Meyer-Pittroff, R.; Hasse, H. Thermodynamic Models for Vapor-Liquid Equilibria of Nitrogen+Oxygen+Carbon Dioxide at Low Temperatures *Cryogenics* **2009**, *49*, 72.

[16] Vrabec, J.; Huang, Y.-L.; Hasse, H. Molecular models for 267 binary mixtures validated by vapor-liquid equilibria: a systematic approach. *Fluid Phase Equilib.* **2009**, available online.

[17] Huang, Y.-L.; Vrabec, J.; Hasse, H. Prediction of ternary vapor-liquid equilibria for 33 systems by molecular simulation. *J. Phys. Chem. B* **2009**, submitted.

[18] Vrabec, J.; Kumar, A.; Hasse, H. Joule-Thomson inversion curves of mixtures by molecular simulation in comparison to advanced equations of state: natural gas as an example. *Fluid Phase Equilib.* **2007**, *258*, 34.

[19] Fernandez, G. A.; Vrabec, J.; Hasse, H. Shear Viscosity and Thermal Conductivity of Quadrupolar Real Fluids from Molecular Simulation. *Mol. Sim.* **2005**, *31*, 787.

[20] Fernandez, G. A.; Vrabec, J.; Hasse, H. Self-Diffusion and Binary Maxwell-Stefan Diffusion Coefficients of Quadrupolar Real Fluids from Molecular Simulation. *Int. J. Thermophys.* **2005**, *26*, 1389.

[21] Müller, E. A. Adsorption of super greenhouse gases on microporous carbons. *Environ. Sci. Tech.* **2005**, *39*, 8736.

[22] Curbelo, S.; Müller, E. A. Modeling of Ethane/Ethylene Separation using Microporous Carbon. *Adsorp. Sci. Tech.* **2005**, *23*, 855.

[23] Müller, E. A. Staggered alignment of quadrupolar molecules inside carbon nanotubes. *J. Phys. Chem. B* **2008**, *112*, 8999.

[24] Cruz, F. J. A. L.; Müller, E. A. Behavior of Ethylene/Ethane Binary Mixtures within Single-Walled Carbon Nanotubes. 1-Adsorption and Equilibrium Properties. *Adsorption* **2009**, *15*, 1.

[25] Allen, M. P.; Tildesley, D. J. *Computer Simulation of Liquids*; Clarendon Press: Oxford, 1987.

[26] Schnabel, T.; Vrabec, J.; Hasse, H. Unlike Lennard-Jones parameters for vapor-liquid equilibria. *J. Mol. Liq.* **2007**, *135*, 170.

[27] Vrabec, J.; Hasse, H. Grand Equilibrium: vapour-liquid equilibria by a new molecular simulation method. *Mol. Phys.* **2002**, *100*, 3375.

[28] Narinskii, G. B. Investigation of the vapor-liquid equilibrium in the system oxygen-argon-nitrogen. I. Experimental data. *Zh. Fiz. Khim.* **1969**, *43*, 408.

[29] Kunz, O.; Klimek, R.; Wagner, W.; Jaschke, M. *The GERG-2004 Wide-Range Reference Equation of State for Natural Gases and Other Mixtures*; Fortschr.-Berichte; VDI-Verlag: Düsseldorf, 2004.

[30] Lemmon, E. W.; Jacobsen, R. T.; Penoncello, S. G.; Friend, D. G. Thermodynamic properties of air and mixtures of nitrogen, argon, and oxygen from 60 to 2000 K at pressures to 2000 MPa. *J. Phys. Chem. Ref. Data* **2000**, *29*, 1.

[31] Frenkel, D.; Smit, B. *Understanding Molecular Simulation: From Algorithms to Applications*; Academic Press: San Diego, 2002.

[32] Escobedo, F. A. Novel pseudoensembles for simulation of multicomponent phase equilibria. *J. Chem. Phys.* **1998**, *108*, 8761.

[33] Escobedo, F. A. Simulation and extrapolation of coexistence properties with single-phase and two-phase ensembles. *J. Chem. Phys.* **2000**, *113*, 8444.

[34] Mehta, M.; Kofke, D. A. Coexistence diagrams of mixtures by molecular simulation. *Chem. Eng. Sci.* **1994**, *49*, 2633.

[35] Watanabe, K. *Guideline on the Henry's Constant and Vapor-Liquid Distribution Constant for Gases in H2O and D2O at High Temperatures*; The International Association for the Properties of Water and Steam: Kyoto, 2004.

[36] Shevkunov, S. V.; Martinovski, A. A.; Vorontsov-Velyaminov, P. N. Calculation of the critical sizes and properties of microdrops using the Monte-Carlo method in a generalized ensemble. *High Temp. Phys. (USSR)* **1988**, *26*, 246.

[37] Nezbeda, I.; Kolafa, J. A New Version of the Insertion Particle Method for Determining the Chemical Potential by Monte Carlo Simulation. *Mol. Sim.* **1991**, *5*, 391.

[38] Vrabec, J.; Kettler, M.; Hasse, H. Chemical potential of quadrupolar two-centre Lennard-Jones fluids by gradual insertion. *Chem. Phys. Lett.* **2002**, *356*, 431.

[39] Lotfi, A.; Vrabec, J.; Fischer, J. Vapour liquid equilibria of the Lennard-Jones fluid from the NpT plus test particle method. *Mol. Phys.* **1992**, *76*, 1319.

[40] Jorgensen, W. L.; Chandrasekhar, J. D.; Madura, R. W.; Impey, R. W.; Klein, M. L. Comparison of simple potential functions for simulating liquid water. *J. Chem. Phys.* **1983**, *79*, 926.

[41] Rowley, R. L.; Wilding, W. V.; Oscarson, J. L.; Yang, Y.; Zundel, N. A.; Daubert, T. E.; Danner, R. P. *DIPPR® Data Compilation of Pure Compound Properties*; Design Institute for Physical Properties; AIChE: New York, 2006.

[42] Lísal, M.; Smith, W. R.; Nezbeda, I. Accurate vapour-liquid equilibrium calculations for complex systems using the reaction Gibbs Ensemble Monte Carlo simulation method. *Fluid Phase Equilib.* **2001**, *181*, 127.

[43] Schnabel, T. *Molecular Modeling and Simulation of Hydrogen Bonding Pure Fluids and Mixtures*; PhD Thesis; University of Stuttgart; 2008.

[44] Andersen, H. C. Molecular dynamics simulations at constant pressure and/or temperature. *J. Chem. Phys.* **1980**, *72*, 2384.

[45] Widom, B. Some Topics in the Theory of Fluids. *J. Chem. Phys.* **1963**, *39*, 2808.

[46] Lustig, R. Angle-average for the powers of the distance between two separated vectors. *Mol. Phys.* **1988**, *65*, 175.

[47] Weingerl, U.; Fischer, J. Consideration of dipole-quadrupole interactions in molecular based equations of state. *Fluid Phase Equilib.* **2002**, *202*, 49.

[48] Flyvbjerg, H.; Petersen, H. G. Error Estimates on Averages of Correlated Data. *J. Chem. Phys.* **1989**, *91*, 461.

Table 1: Parameters of the pure substance 2CLJQ molecular models for nitrogen, oxygen, and argon, taken from [13].

pure fluid	σ	ε/k_B	L	Q
	Å	K	Å	DÅ
nitrogen	3.3211	34.897	1.0464	1.4397
oxygen	3.1062	78.020	0.9699	0.8081
argon	3.3952	116.79	—	—

Table 2: Binary interaction parameters ξ, cf. Equation (7), for the three binary subsystems, taken from [11].

mixture	ξ
	—
nitrogen-oxygen	1.007
nitrogen-argon	1.008
oxygen-argon	0.988

Table 3: Density and residual internal energy of dry air along three isotherms. The number in parentheses indicates the statistical uncertainty in the last digit.

p MPa	ρ mol/l	u^{res} kJ/mol
$T = 293.15$ K		
2	0.825(1)	-0.117(1)
5	2.069(1)	-0.293(1)
10	4.127(3)	-0.581(1)
15	6.100(5)	-0.854(1)
20	7.936(7)	-1.109(1)
25	9.568(9)	-1.334(2)
40	13.48 (1)	-1.872(2)
60	16.979(9)	-2.344(2)
100	21.22 (2)	-2.901(4)
150	24.45 (2)	-3.280(3)
200	26.68 (2)	-3.507(3)
$T = 353.15$ K		
2	0.6792(4)	-0.0910(4)
5	1.690 (1)	-0.227 (1)
10	3.328 (2)	-0.445 (1)
15	4.888 (3)	-0.652 (1)
20	6.356 (5)	-0.847 (1)
25	7.707 (5)	-1.022 (1)
40	11.120 (8)	-1.471 (2)
60	14.49 (1)	-1.909 (2)
100	18.876 (9)	-2.457 (2)
150	22.34 (2)	-2.853 (3)
200	24.71 (1)	-3.082 (3)
$T = 473.15$ K		
2	0.505(1)	-0.0623(3)
5	1.247(1)	-0.1521(4)
10	2.440(1)	-0.300 (1)
15	3.576(2)	-0.438 (1)
20	4.655(2)	-0.568 (1)
25	5.675(3)	-0.693 (1)
40	8.369(5)	-1.015 (1)
60	11.279(6)	-1.361 (1)
100	15.497(7)	-1.843 (2)
150	19.06 (2)	-2.219 (3)
200	21.60 (2)	-2.446 (4)

Table 4: Density and residual internal energy of dry air along three isobars. The number in parentheses indicates the statistical uncertainty in the last digit.

T	ρ	u^{res}
K	mol/l	kJ/mol
$p = 2$ MPa		
213.15	1.168 (1)	-0.186 (1)
233.15	1.055 (1)	-0.161 (1)
253.15	0.964 (1)	-0.1430(5)
273.15	0.889 (1)	-0.1298(5)
293.15	0.825 (1)	-0.117 (1)
313.15	0.769 (1)	-0.1086(4)
333.15	0.722 (1)	-0.0983(4)
353.15	0.6792(4)	-0.0910(4)
373.15	0.642 (1)	-0.0848(4)
393.15	0.609 (1)	-0.0792(3)
413.15	0.579 (1)	-0.0738(3)
473.15	0.5047(2)	-0.062 (1)
573.15	0.4160(2)	-0.0484(4)
773.15	0.3086(2)	-0.0309(4)
973.15	0.2455(1)	-0.0218(4)
1273.15	0.1878(1)	-0.0133(3)
$p = 10$ MPa		
213.15	6.493 (8)	-0.995 (2)
233.15	5.607 (5)	-0.842 (1)
253.15	4.985 (4)	-0.731 (1)
273.15	4.504 (3)	-0.647 (1)
293.15	4.127 (3)	-0.581 (1)
313.15	3.814 (2)	-0.528 (1)
333.15	3.555 (2)	-0.483 (1)
353.15	3.328 (2)	-0.445 (1)
373.15	3.131 (2)	-0.413 (1)
393.15	2.962 (1)	-0.383 (1)
413.15	2.809 (1)	-0.361 (1)
473.15	2.442 (2)	-0.297 (1)
573.15	2.010 (1)	-0.230 (1)
773.15	1.497 (1)	-0.151 (1)
973.15	1.193 (1)	-0.105 (1)
1273.15	0.9176(3)	-0.064 (1)
$p = 25$ MPa		
213.15	14.62 (2)	-2.181 (2)
233.15	12.89 (2)	-1.889 (2)
253.15	11.54 (1)	-1.661 (2)
273.15	10.45 (1)	-1.480 (2)
293.15	9.568 (9)	-1.334 (2)
313.15	8.836 (7)	-1.213 (1)
333.15	8.235 (6)	-1.113 (1)
353.15	7.707 (5)	-1.022 (1)
373.15	7.259 (5)	-0.950 (1)
393.15	6.868 (5)	-0.888 (1)
413.15	6.519 (4)	-0.829 (1)
473.15	5.664 (7)	-0.690 (2)
573.15	4.694 (4)	-0.537 (1)
773.15	3.530 (2)	-0.353 (1)
973.15	2.839 (2)	-0.249 (1)
1273.15	2.202 (1)	-0.153 (1)

Table 5: Parameters of the molecular models for water, cf. Figure 7. The electronic charge is $e = 1.6021 \cdot 10^{-19}$ C.

water model	r_{OH} Å	α °	δ Å	σ Å	$\varepsilon/k_{\mathrm{B}}$ K	q e
TIP4P [40]	0.9572	104.52	0.15	3.15365	78.02	0.52
new model	0.9670	104.52	0.15004	3.31500	95.646	0.52748

Table 6: Density of compressed humid air from simulation in comparison to experimental data [10]. Here, the statistical uncertainty of the density is denoted by $\delta\rho$, whereas $\Delta\rho = \rho_{\mathrm{sim}} - \rho_{\mathrm{exp}}$.

T K	p MPa	x_{W} mol/mol	ρ_{exp} mol/l	ρ_{sim} mol/l	$\delta\rho_{\mathrm{sim}}$ mol/l	$\Delta\rho/\rho_{\mathrm{exp}}$ %	$\delta\rho_{\mathrm{sim}}/\rho_{\mathrm{exp}}$ %
TIP4P model							
424.11	10.877	0.0420	3.020	2.980	0.006	-1.34	0.21
524.33	13.684	0.0420	3.004	2.965	0.008	-1.27	0.27
498.40	8.892	0.0446	2.124	2.074	0.009	-2.39	0.43
498.41	4.388	0.0445	1.064	1.042	0.002	-2.04	0.20
423.30	13.747	0.0126	3.727	3.697	0.008	-0.81	0.23
515.56	17.045	0.0126	3.708	3.702	0.009	-0.16	0.24
new water model							
424.11	10.877	0.0420	3.020	2.974	0.011	-1.52	0.37
524.33	13.684	0.0420	3.004	2.970	0.008	-1.12	0.27
498.40	8.892	0.0446	2.124	2.073	0.006	-2.41	0.27
498.41	4.388	0.0445	1.064	1.041	0.003	-2.14	0.29
423.30	13.747	0.0126	3.727	3.701	0.010	-0.70	0.26
515.56	17.045	0.0126	3.708	3.694	0.008	-0.38	0.22

Table 7: Vapor-liquid equilibria of the water models: vapor pressure, saturated densities, and enthalpy of vaporization. The number in parentheses indicates the statistical uncertainty in the last digit.

T K	p_{W}^{σ} MPa	ρ_{W}' mol/l	ρ_{W}'' mol/l	$\Delta h_{\mathrm{W}}^{\mathrm{v}}$ kJ/mol
TIP4P				
333.15	0.045(3)	53.90(5)	0.0169(9)	40.6(2)
353.15	0.100(3)	52.93(4)	0.0355(9)	39.4(3)
new water model				
333.15	0.015(1)	55.21(5)	0.0053(4)	45.3(2)
353.15	0.042(2)	54.53(6)	0.0146(7)	44.1(3)

Table 8: Dew point, vapor concentration enhancement factor g_{W}, and vapor pressure enhancement factor f_{W} of humid air. The numbers in parentheses indicate the statistical uncertainty in the last digits.

T	p	ρ	x_{W}	g_{W}	f_{W}
K	MPa	mol/l	mol/mol	—	—
TIP4P					
333.15	2.0	0.7223(2)	0.0238(2)	1.02(6)	1.05(7)
	5.0	1.7992(7)	0.0103(1)	1.10(7)	1.13(8)
	10.0	3.557(1)	0.00594(8)	1.25(8)	1.30(9)
	15.0	5.231(2)	0.00456(9)	1.42(10)	1.51(11)
	20.0	6.799(3)	0.00403(7)	1.63(12)	1.78(13)
	22.5	7.538(3)	0.00373(8)	1.67(13)	1.85(14)
	25.0	8.239(3)	0.0040(1)	1.93(11)	2.18(13)
353.15	2.0	0.6814(2)	0.0529(4)	1.02(4)	1.06(4)
	5.0	1.6925(6)	0.0232(2)	1.10(4)	1.16(4)
	10.0	3.334(1)	0.0132(2)	1.24(5)	1.33(5)
	15.0	4.899(2)	0.0105(2)	1.45(6)	1.58(6)
	20.0	6.367(3)	0.0091(2)	1.64(7)	1.83(8)
	22.5	7.064(3)	0.0089(2)	1.78(9)	2.02(10)
	25.0	7.730(4)	0.0082(2)	1.79(9)	2.06(10)
new water model					
333.15	2.0	0.7219(2)	0.0075(1)	1.02(8)	1.00(8)
	5.0	1.7983(5)	0.00333(4)	1.13(9)	1.11(9)
	10.0	3.555(1)	0.00191(2)	1.28(10)	1.27(10)
	15.0	5.226(2)	0.00144(2)	1.42(12)	1.44(12)
	20.0	6.798(3)	0.00124(2)	1.59(13)	1.65(14)
	22.5	7.531(4)	0.00117(2)	1.66(14)	1.76(14)
	25.0	8.232(4)	0.00117(4)	1.82(18)	1.95(19)
353.15	2.0	0.6800(2)	0.0217(2)	1.01(6)	1.03(6)
	5.0	1.6902(5)	0.0094(1)	1.08(7)	1.12(7)
	10.0	3.330(1)	0.00538(7)	1.23(8)	1.28(8)
	15.0	4.895(2)	0.00416(7)	1.39(9)	1.49(9)
	20.0	6.361(3)	0.00358(8)	1.56(11)	1.70(12)
	22.5	7.050(4)	0.00338(8)	1.63(12)	1.81(13)
	25.0	7.720(4)	0.0034(1)	1.80(16)	2.03(17)

List of Figures

1 Vapor-liquid equilibrium of the ternary system nitrogen + oxygen + argon at 120 K and 1.995 MPa. Present simulation results (●) are compared to experimental data [28] (+) and the GERG-2004 EOS [29] (—). The numbers indicate the predicted vapor pressure. 30

2 Density of dry air (top) and relative deviation to the GERG-2004 EOS [29] (bottom). Present simulation results: ● 2 MPa, ▲ 10 MPa, and ■ 20 MPa. — GERG-2004 EOS, – – EOS by Lemmon et al. [30]. 31

3 Density of dry air (top) and relative deviation to the GERG-2004 EOS [29] (bottom). Present simulation results: ● 293.15 K, ▲ 353.15 K, and ■ 473.15 K. — GERG-2004 EOS, – – EOS by Lemmon et al. [30]. 32

4 Residual energy of dry air (top) and relative deviation to the GERG-2004 EOS [29] (bottom). Present simulation results: ● 2 MPa, ▲ 10 MPa, and ■ 20 MPa. — GERG-2004 EOS, – – EOS by Lemmon et al. [30]. 33

5 Residual energy of dry air (top) and relative deviation to the GERG-2004 EOS [29] (bottom). Present simulation results: ● 293.15 K, ▲ 353.15 K, and ■ 473.15 K. — GERG-2004 EOS, – – EOS by Lemmon et al. [30]. 34

6 Running average of total molar density (top) and water mole fraction (bottom) during the course of Mollier simulation of humid air with the TIP4P water model at 333.15 K and 5 MPa. Note that the loop counter was initialized at the end of equilibriation. 35

7 Molecular model for water. The LJ site is located at the oxygen nucleus, denoted by O. The partial charges are denoted by bullets. At the hydrogen nuclei, denoted by H, two positive charges $+q$ are located. The negative charge $-2q$ is shifted by δ towards the hydrogen nuclei and located at the site denoted by M. 36

8 Saturated densities of pure water: ● simulation results from new model, this work, ▲ simulation results from TIP4P model [42], — correlation to experimental data [41], ○ critical point from simulation (new model), + experimental critical point. 37

9 Vapor pressure of pure water: ● simulation results from new model, this work, ▲ simulation results from TIP4P model [42], — correlation to experimental data [41], ○ critical point from simulation (new model), + experimental critical point. 38

10 Enthalpy of vaporization of pure water: ● simulation results from new model, this work, ▲ simulation results from TIP4P model [42], — correlation to experimental data [41]. 39

11 Relative deviations of vapor-liquid equilibrium properties between simulation data and correlations to experimental data for pure water [41] ($\delta z = (z_{\mathrm{sim}} - z_{\mathrm{exp}})/z_{\mathrm{exp}}$): ● new model, this work, ▲ TIP4P model [42]. Top: vapor pressure, center: saturated liquid density, bottom: enthalpy of vaporization. 40

12 Illustration of the Mollier ensemble. 41

13 Vapor pressure enhancement factor f_{W}. Present simulation results obtained with different water models: ● new model, ▲ TIP4P model, — correlation of Wylie and Fisher [6], – – GERG-2004 EOS [29]. 42

14 Concentration enhancement factor g_{W}. Present simulation results obtained with different water models: ● new model, ▲ TIP4P model, ○ experimental results from Koglbauer and Wendland [7], — prediction of Wylie and Fisher [6], – – GERG-2004 EOS [29]. 43

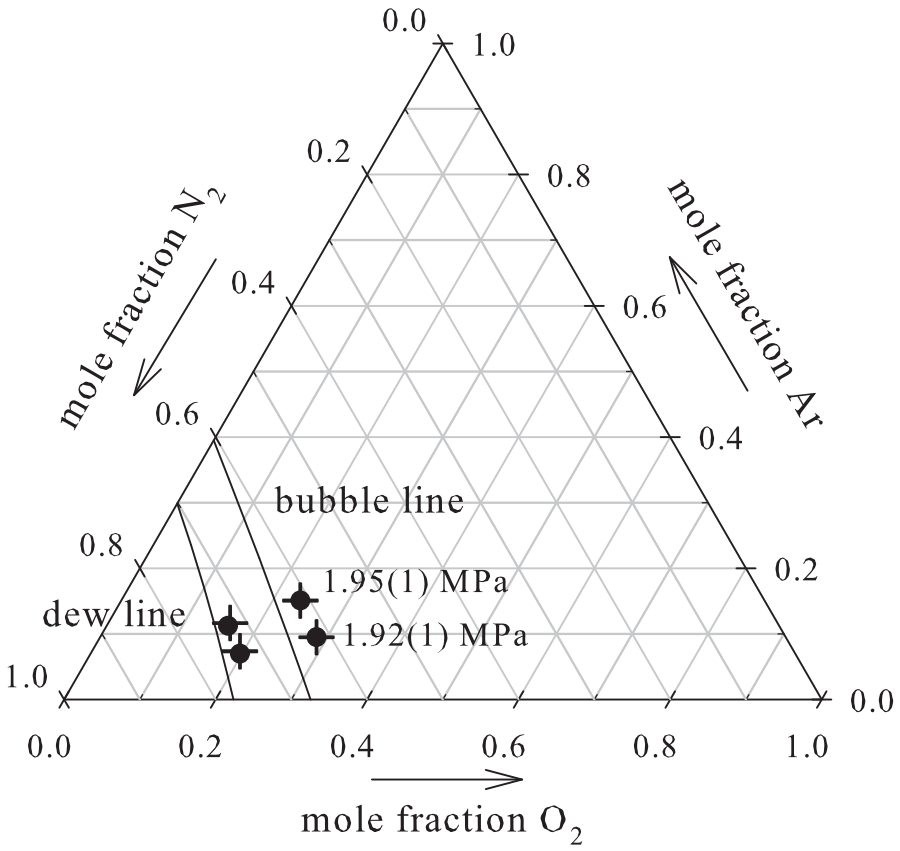

Figure 1: Eckl et al.

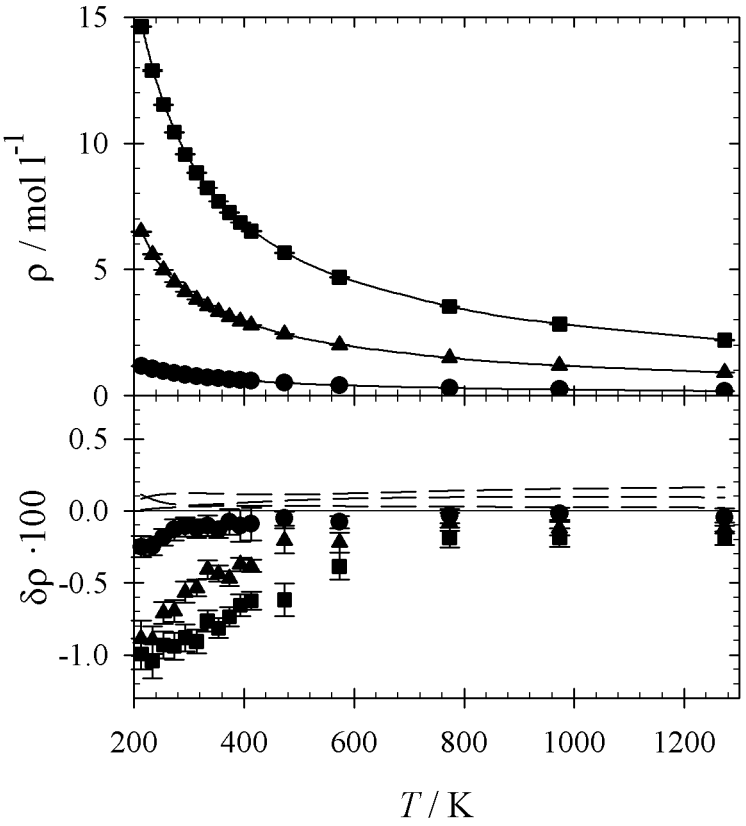

Figure 2: Eckl et al.

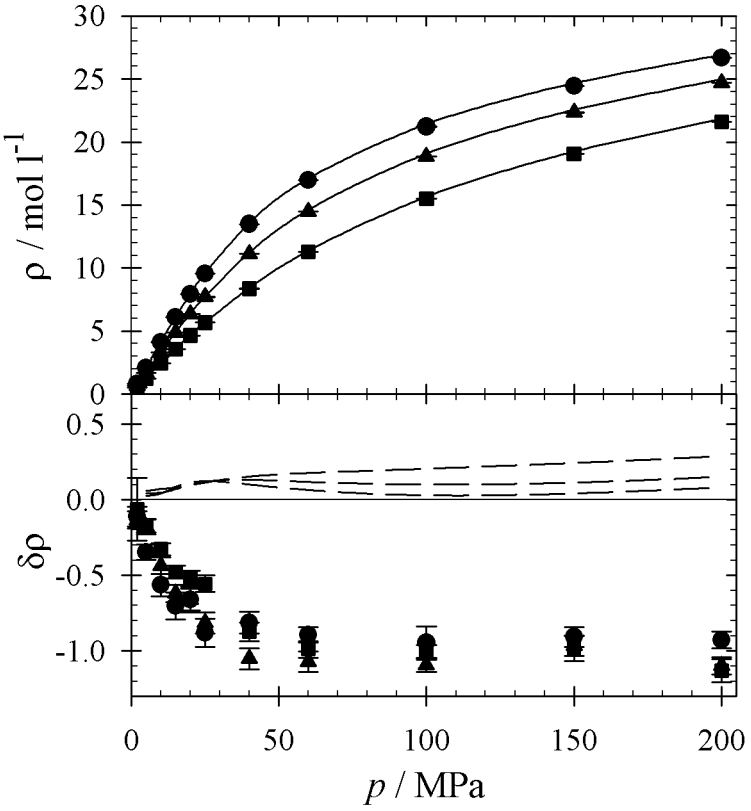

Figure 3: Eckl et al.

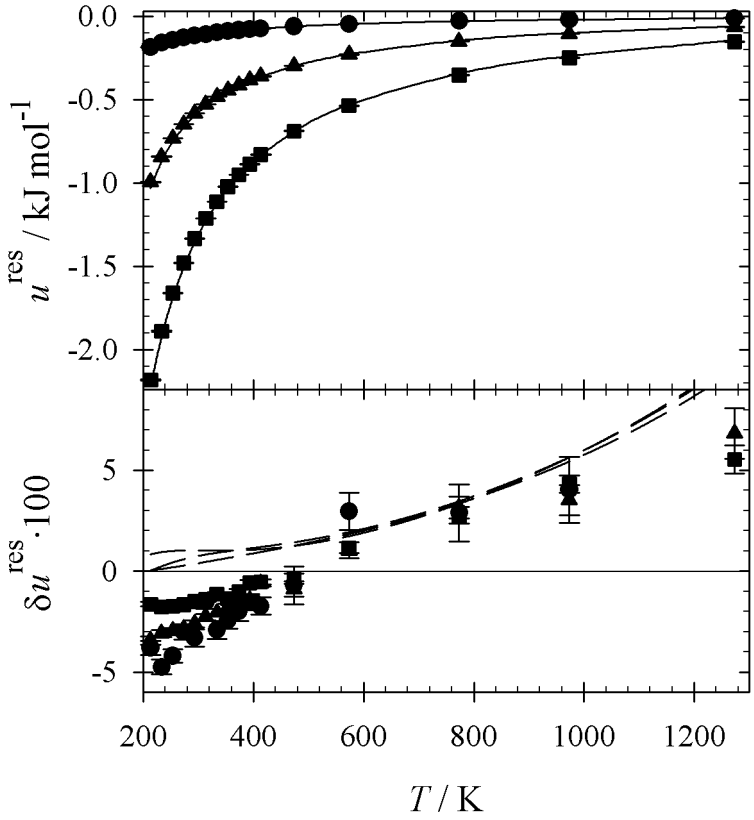

Figure 4: Eckl et al.

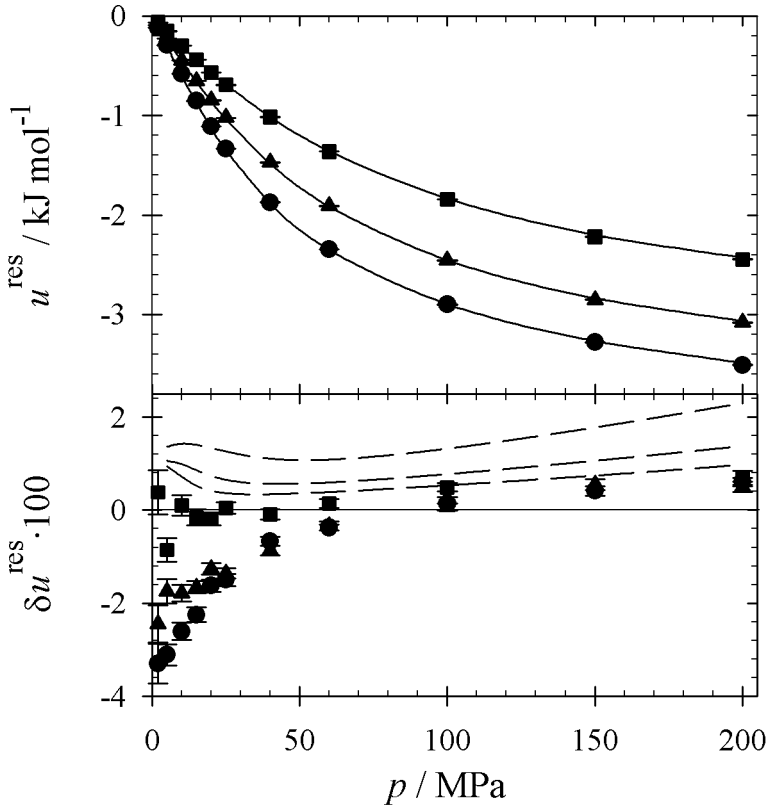

Figure 5: Eckl et al.

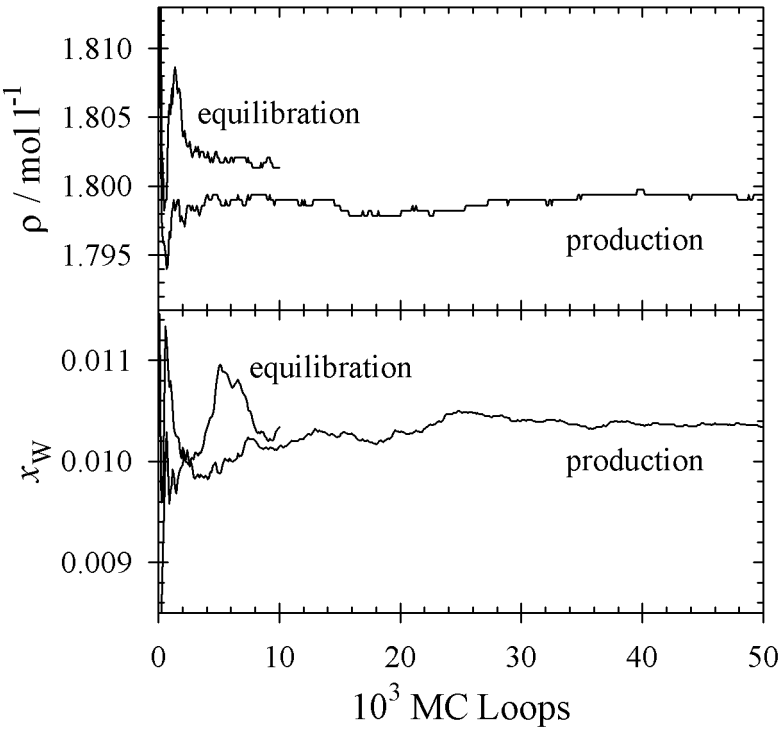

Figure 6: Eckl et al.

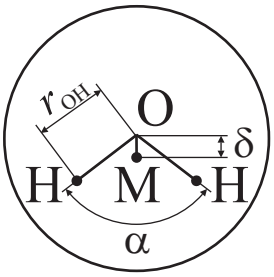

Figure 7: Eckl et al.

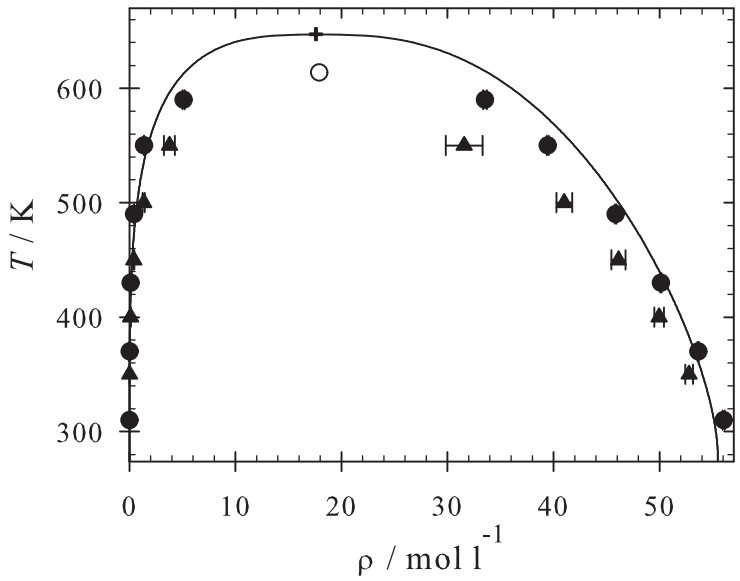

Figure 8: Eckl et al.

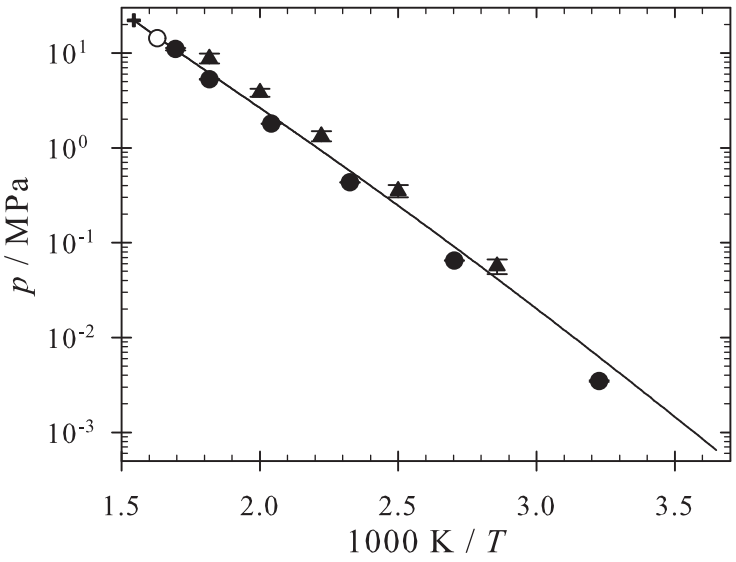

Figure 9: Eckl et al.

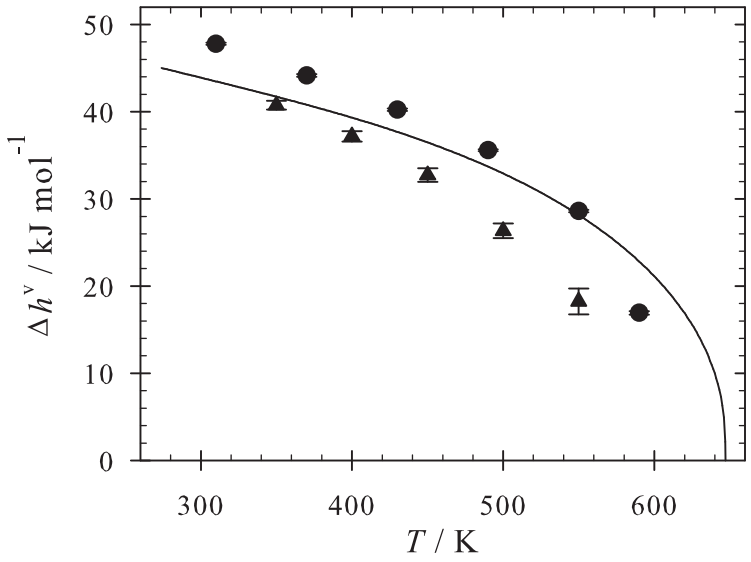

Figure 10: Eckl et al.

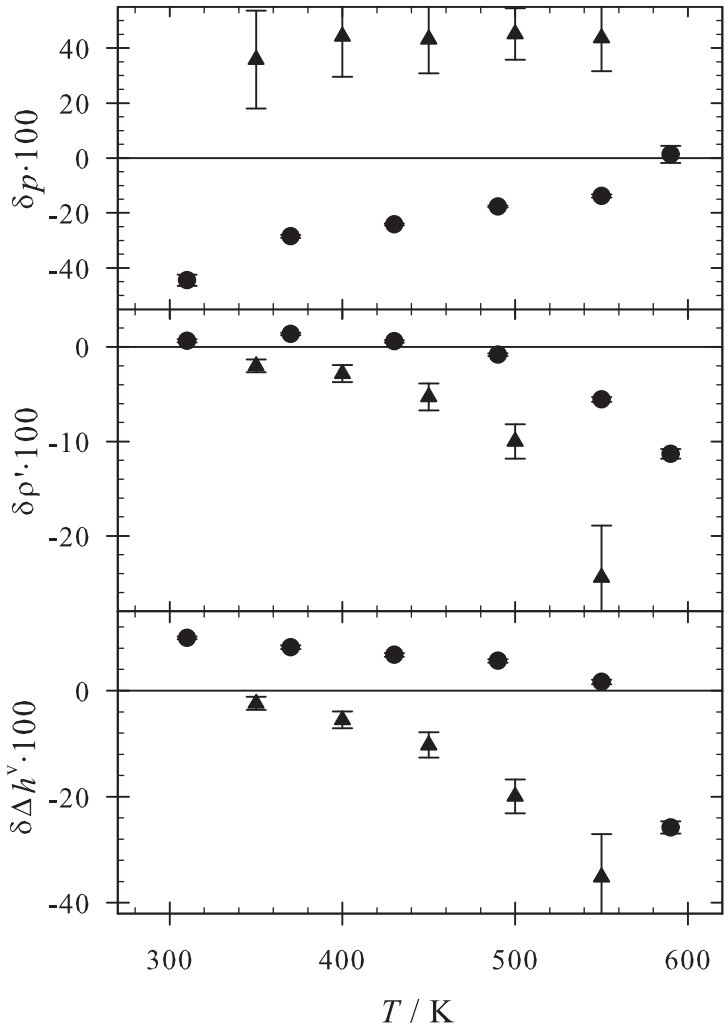

Figure 11: Eckl et al.

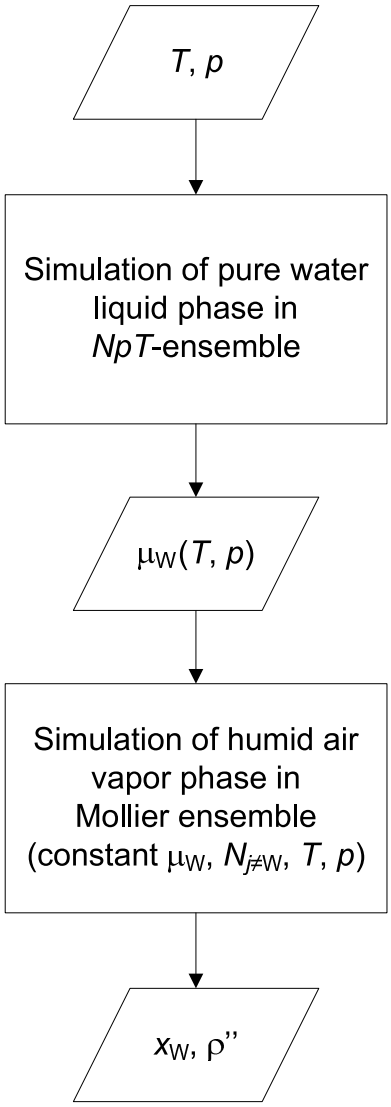

Figure 12: Eckl et al.

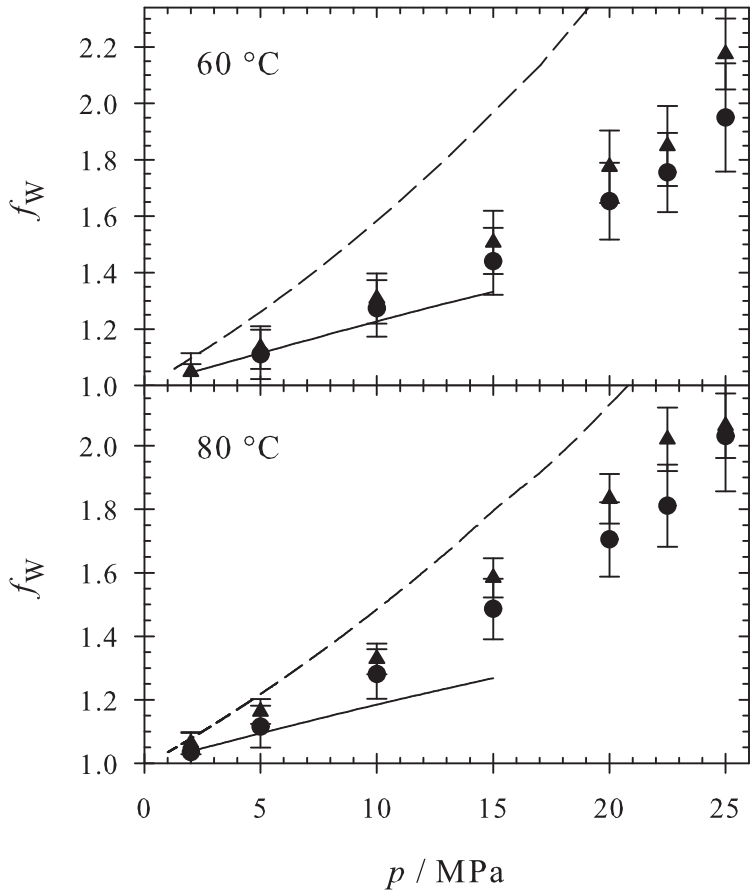

Figure 13: Eckl et al.

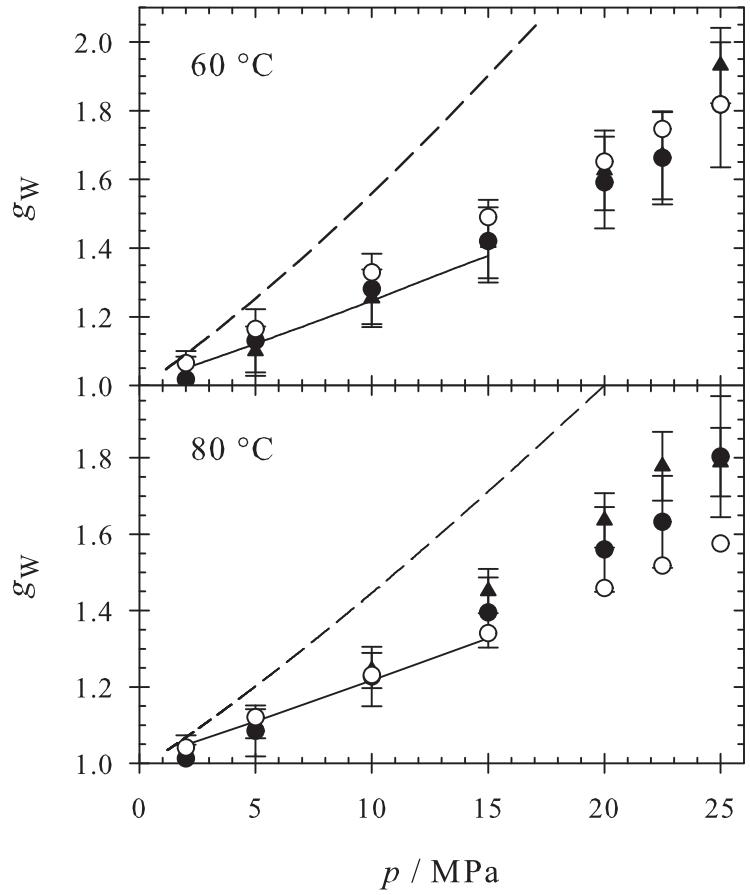

Figure 14: Eckl et al.